Human Molecular Genetics, 2015, Vol. 24, No. 13 3679–3688

doi: 10.1093/hmg/ddv111
Advance Access Publication Date: 25 March 2015
Original Article

ORIGINAL ARTICLE

Crucial role of posttranslational modifications of integrin α3 in interstitial lung disease and nephrotic syndrome

Ebru G. Yalcin[1,†], Yinghong He[3,†], Diclehan Orhan[2], Chiara Pazzagli[3,4], Nagehan Emiralioglu[1] and Cristina Has[3,*]

[1]Department of Pediatric Pulmonology and [2]Department of Pediatric Pathology, Hacettepe University Faculty of Medicine, Ankara, Turkey, [3]Department of Dermatology, Medical Center, University of Freiburg, Freiburg, Germany and [4]Spemann Graduate School of Biology and Medicine (SGBM), Albert Ludwigs University Freiburg, Freiburg, Germany

*To whom correspondence should be addressed at: Department of Dermatology, Medical Center, University of Freiburg, Hauptstrasse 7, 79104 Freiburg, Germany. Tel: +49 76127069920; Fax: +49 76127067200; Email: cristina.has@uniklinik-freiburg.de

Abstract

Interstitial lung disease, nephrotic syndrome and junctional epidermolysis bullosa is an autosomal recessive multiorgan disorder caused by mutations in the gene for the integrin α3 subunit (*ITGA3*). The full spectrum of manifestations and genotype–phenotype correlations is still poorly characterized. Here, we uncovered the disease-causing role and the molecular mechanisms underlying a homozygous *ITGA3* mutation leading to the single amino acid substitution, p.R463W. The patient suffered from respiratory distress and episodes of cyanosis with onset in the first week of life and had a nephrotic syndrome. Although there was no clinical evidence for cutaneous fragility, the analysis of a skin sample and of skin epithelial cells enabled the direct assessment of the authentic mutant protein. We show that the mutation altered the conformation of the extracellular β-propeller domain of the integrin α3 subunit preventing correct processing of N-linked oligosaccharides, heterodimerization with β1 integrin and maturation through cleavage into heavy and light chains in the Golgi. Confocal microscopy demonstrated that the mutant protein accumulated intracellularly, but it was not present in focal adhesions or on the cell membrane as shown by flow cytometry. These findings highlight that single amino acid changes in the integrin α3 subunit may crucially alter the structure and complex processing of this integrin, completely preventing its functionality. The present report also underscores that *ITGA3* mutations may account for atypical cases solely with early onset respiratory and renal involvement.

Introduction

Loss-of-function mutations of the integrin α3 subunit were recently associated with interstitial lung disease, nephrotic syndrome and junctional epidermolysis bullosa (ILNEB, OMIM 614748) in four cases (1,2) (Table 1); nonetheless, the genotype–phenotype correlations and the underlying disease mechanisms remained largely unknown. Integrins are transmembrane αβ glycoproteins that connect the extracellular matrix to the cytoskeleton. Most integrins connect to actin filaments and reside in cellular adhesion structures designated as focal adhesions, which are highly enriched in tyrosine-phosphorylated proteins and serve as major hubs for signal transduction (5). By integrating the extracellular environment with the cell interior, integrin

[†]These authors contributed equally.

Received: January 22, 2015. **Revised and Accepted:** March 23, 2015

Table 1. Summary of pulmonary, renal and cutaneous features in reported ILNEB cases

Cases integrin α3 *Mutation* (cDNA and protein) *Phenotype* (including age of onset and additional features)	Lung - Respiratory distress - Oxygen dependent - Infections - CT /biopsy: interstitial lung disease	Kidney Congenital nephrotic syndrome	Skin - Blisters - Persistent erosions - Nail dystrophy - Sparse hair	Demise	Reference
1	At birth	Day 13	3 months	7.5 months of respiratory infection	(1)
c.1173_1174del	+	+	+		
p.P392V*fs**	+	Hypoplastic kidney	+		
	+		+		
	+		+		
2	Day 2	6 weeks	1.5 months	2 months of multiple organ failure	(1,3)
c.1538-1G>A	+	+	+		
	+	Renal hypodysplasia	+		
	+		–		
	+		–		
3	2 months	2 months	4 months	19 months of multiorgan failure related to infection	(1,4)
c.1883G>C	+	+	+		
p.R628P	+	Focal-segmental glomerulosclerosis	–		
	+		+		
	+		–		
4	At birth	NA		7 months of respiratory insufficiency	(2)
c.1045G>T	+	+	–		
p.A349S	Na	Unilateral kidney hypoplasia with hydronephrosis on the left side	–		
	Na		–		
	Na		–		
5	Day 7	6 weeks	5 months	6.5 months of respiratory infection	This study
c.1387C>T	+	+	–		
p.R463W	+	crossed fused renal ectopia	–		
	+		+		
	+		+		

+, feature present; –, feature absent; Na, information not available.

receptors also control cell survival, proliferation and differentiation, and display unique and redundant functions in tissues (6), rendering the molecular disease mechanisms highly complex.

Integrin α3 subunit is widely expressed in epithelia, including lung epithelium, in kidney podocytes and skin epidermis (7). Initially, constitutive and organ-specific knockout mouse models shed light on the consequences of loss of this subunit *in vivo*. Integrin α3 knockout mice die within 24 h after birth, because of defects in kidney and/or lung organogenesis (8). They demonstrate abnormalities of the renal architecture regarding the formation of the collecting system, the proper growth and maintenance of proximal tubules and the capillary loops. Podocytes fail to differentiate are decreased in number and demonstrate a dramatic absence of foot process formation (8). Mice with podocyte specific deletion of *Itga3* display similar anomalies—foot process effacement, severe proteinuria and end-stage renal disease (9). In contrast, deletion of the α3 subunit exclusively in the developing collecting duct resulted in only a mild developmental phenotype (9). Mice with cell-specific loss of integrin α3 in alveolar epithelial cells had grossly preserved alveolar architecture and normal total lung capacity and airway resistance; in this model, α3 deficiency prevented the progression of fibrosis after bleomycin treatment (10). Finally, the constitutive and epidermal-specific *Itga3* knockout mice display microblistering at the dermal–epidermal junction and basement membrane (BM) duplication (11–13). In the skin of these mice, loss of integrin α3 affects proper organization and stabilization of the epidermal BM (11,13), but not epidermal morphogenesis (14,15).

Here, we uncovered the disease-causing role of a single amino acid substitution, p.R463W, in the extracellular β-propeller domain of integrin α3 in a patient with fatal lung disease and congenital nephrotic syndrome, and demonstrate that defective posttranslational modification of integrin α3 prevents its incorporation and function at the cell membrane. Illumination of the biological consequences of this naturally occurring human mutation contributes to the understanding of the function and structure of integrin α3.

Results

Clinical and morphological findings

A 14-day-old male patient was admitted to hospital with respiratory distress and episodes of cyanosis. The child was born at 40 weeks of pregnancy, with no health complications, weighing 3000 g, and was discharged from the hospital at the same time as his mother. Seven days after delivery, respiratory distress and episodes of cyanosis developed and he was referred to our department because of respiratory distress requiring continuous oxygen. The parents reported second degree consanguinity.

Physical examination detected pallor and poor weight gain, and tachypnea with a respiratory rate of 64 min^{-1} and intercostal retraction. Transcutaneous oxygen saturation was 84% in room

air and respiratory auscultation detected bilateral crepitation. Results of full blood counts were within normal range. Chest radiography showed bilateral diffuse interstitial infiltrates (Fig. 1A). Although he received ampicillin and gentamycin because of suspected congenital pneumonia, clinical findings were not improved. Chest computed tomography revealed diffuse ground glass opacity and interlobular septal thickening consistent with diffuse interstitial lung disease (Fig. 1B). *Mycoplasma pneumonia* and *Chlamydia pneumonia* serology was negative. Flexible bronchoscopy did not reveal any pathological findings. Cytomegalovirus (CMV) polymerase chain reaction (PCR) in bronchoalveolar lavage fluid was 512 copies/ml; however, the blood CMV PCR was negative. Immunoglobulins and lymphocyte subsets were in normal range. Laboratory tests at 6 weeks of age indicated nephrotic-range proteinuria and hypoalbuminemia. Abdominal ultrasonography showed crossed fused renal ectopia. Blood and urine culture were negative.

Broad-spectrum antibiotic and antifungal therapies and ganciclovir were used to treat pneumonia, but there was no improvement of the clinical and radiological findings. Lung biopsy was performed at the age of 2 months and revealed abnormal alveolarization, manifesting as enlarged, round and poorly septated ('simplified') alveolar spaces (Fig. 2A). This finding was consistent with alveolar growth disorder. Some other areas showed thickening of interalveolar septa and there was one pneumocyte with CMV inclusion (Fig. 2B). During the clinical observation, he developed severe respiratory distress and required endotracheal intubation and mechanical ventilation for 2 weeks, from which he was successfully weaned. Laboratory tests at 3 months of the age indicated nephrotic-range proteinuria again. Renal biopsy was planned, but it was not performed because of crossed fused renal ectopia. Respiratory distress persisted during his follow-up and he required supplemental oxygen to maintain oxygen saturation values at a level >90%.

Methylprednisolone treatment was started at 2 mg/kg/day due to suspicion of interstitial lung disease, as there was no improvement, the steroid therapy was tapered day by day. From the age of 5 months, the infant had fine sparse scalp hair, mild thickening of the toenails (Fig. 3A) and growth retardation.

All these clinical, radiological and pathological findings suggested an integrin α3-associated disease. After informed consent, skin biopsy and EDTA-blood were obtained and submitted to molecular diagnostics, and he was discharged from the hospital at the age of 6 months with oxygen treatment. After hospital discharge, the infant died at the age of 6.5 months during an episode of pulmonary infection at another center.

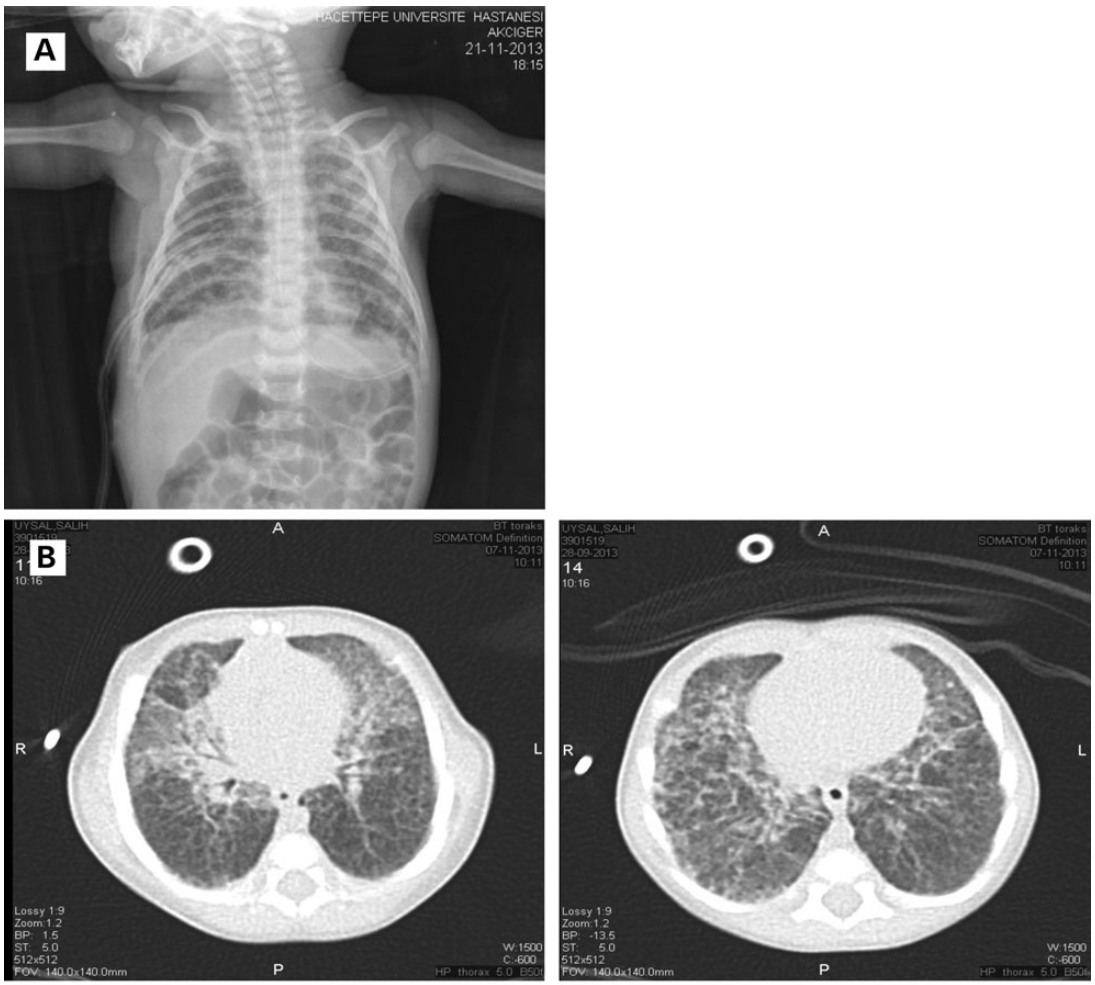

Figure 1. Radiological findings. (**A**) Chest radiography showed bilateral diffuse interstitial infiltrates at the age of 1.5 months. (**B**) Chest CT at the age of 1.5 months revealed diffuse ground glass opacity and interlobular septal thickening consistent with diffuse interstitial lung disease.

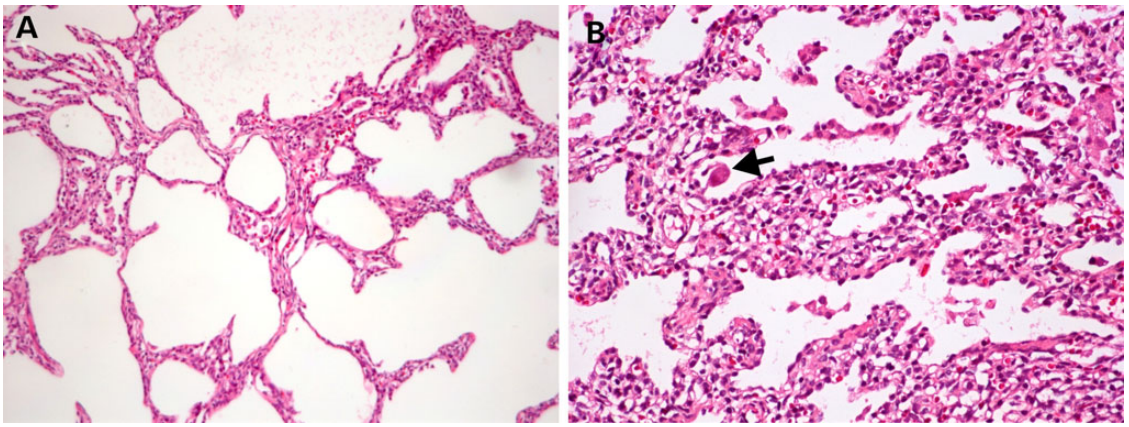

Figure 2. Lung histological findings. (**A**) Lung biopsy was performed at the age of 2 months showing alveolar simplification in most of the areas (HE, original magnification ×100). (**B**) Focal areas revealing thickening of the interalveolar septa with a pneumocyte showing cytomegalovirus inclusion (arrow) (HE, original magnification ×200).

Disease-causing mutation and its biological consequences

To elucidate the underlying molecular defect, the skin biopsy was submitted to immunofluorescence antigen mapping as described before (1). Although clinically, no skin blistering was noticed, a junctional split was observed in the skin sample of the patient, as well as the lack of immunoreactivity for integrin α3 with the antibody P1B5, which stained at the periphery of basal keratinocytes in control skin (Fig. 3B). Immunostaining of integrin α6 was noted at the blister roof in the patient's skin, with a similar intensity as in the control skin (Fig. 3B). Based on these findings, *ITGA3* mutation analysis was performed and a homozygous variant, c.1387C>T, p.R463W (in respect to NM_002204.2, NC_000017.11) was identified in the patient, which was present in a heterozygous state in each of the parents (Fig. 3C). This variant was excluded from 100 control chromosomes and from the single-nucleotide polymorphism database (dbSNP 141) and the Exome variant server. The amino acid substitution affects the conserved arginine 463, in the β-propeller domain of integrin α3 and is predicted to be disease causing (PolyPhen2 score 1, Mutation Taster score 0.90). The tertiary structure of a sequence spanning amino acids 80–481 of wild-type and mutant integrin α3 was modeled (http://scratch.proteomics.ics.uci.edu/) (16), indicating that tryptophan at position 463 significantly alters the conformation of the β-propeller domain (Fig. 3D and E).

To explain the pathogenic role of the identified variant, we analyzed its consequences using patient's skin epithelial cells. Hence, keratinocytes were isolated from the skin biopsy of the patient and a healthy age-matched control, cultured and immortalized with the human papilloma virus genes E6E7, as described before (17). Quantitative real-time PCR with RNA extracted from the subconfluent keratinocytes demonstrated that *ITGA3* mRNA was ∼1.5-fold upregulated in the patient's cells compared with the control cells (Fig. 4A), suggesting that the mutant integrin α3 polypeptide was expressed.

Integrin α3 is synthetized as a precursor of ∼150 kDa (pre-α3A). After N-glycosylation in the endoplasmic reticulum (ER) and association with β1, the α3β1 heterodimer is transported in the Golgi, where processing of N-linked oligosaccharides occurs, and pre-α3A is cleaved into a heavy (115 kDa) and a light chain (35 kDa), which represent the mature form of the molecule (2) (Fig. 3E). Immunoblot analysis using antisera 8-4 B7 which recognize both pre-α3A and the light chain (18) showed that in the patient's keratinocytes, only the precursor was present, but not the mature light chain (Fig. 4B). We next determined the cell surface expression of the α3 and β1 integrin subunits in the patient's keratinocytes by flow cytometry. While no signal for integrin α3 was detected at the surface of the patient's keratinocytes, β1 was not significantly changed compared with the control cells, suggesting that it was still assembled, integrated into the membrane and activated (Fig. 4C). In agreement with these findings, immunofluorescence staining demonstrated the absence of the mutant integrin α3 at vinculin- and integrin β1-positive focal adhesions and its accumulation in the cytoplasm (Fig. 4D). These results demonstrate that mutant integrin α3 is synthetized as a precursor polypeptide, which is not cleaved and is not subsequently targeted to the cell membrane to fulfill its physiological functions. Notably, immunoprecipitation of α3 and β1 integrins showed no association between the mutant integrin α3 and the β1 subunit (Fig. 4F).

In immunoblot under reducing conditions, wild-type pre-α3A appears as two bands (Figs 4B and 5A, D), which likely represent the high-mannose form in the ER, and the complex form after modification of the N-linked oligosaccharides in the Golgi apparatus (2). We reasoned that the absence of the upper band observed in the patient's sample (Fig. 4B) reflects a defect in glycosylation, after excluding a difference in the phosphorylation pattern (not shown). After treatment with *N*-glycanase (PNGase), an enzyme that cleaves between the innermost *N*-acetylglucosamine and asparagine residues of high mannose, hybrid and complex oligosaccharides from N-linked glycoproteins, deglycosylated wild-type and mutant pre-α3A migrated similarly (Fig 5A, left panel). Treatment with tunicamycin, a pharmacological inhibitor of N-glycosylation, generated similar lower bands in both cell types (Fig. 5A, right panel, red arrow); the upper band, which was only present in the control sample and presumably represents a complex processed form, was not changed by this treatment (Fig. 5A, right panel). These results suggest that mutant integrin α3 is N-glycosylated in ER, and that processing of N-linked oligosaccharides in Golgi is impaired, probably due to the influence of the protein conformation on N--linked oligosaccharide processing. Since the proteolytic processing of the heavy and light chains also takes place in the Golgi apparatus (19), it seems likely that the misfolded mutant integrin α3 is either not properly transported from the ER to the Golgi or not further correctly processed in the Golgi. To address this, double immunofluorescence staining for integrin α3 and markers for either ER or Golgi was performed. In the

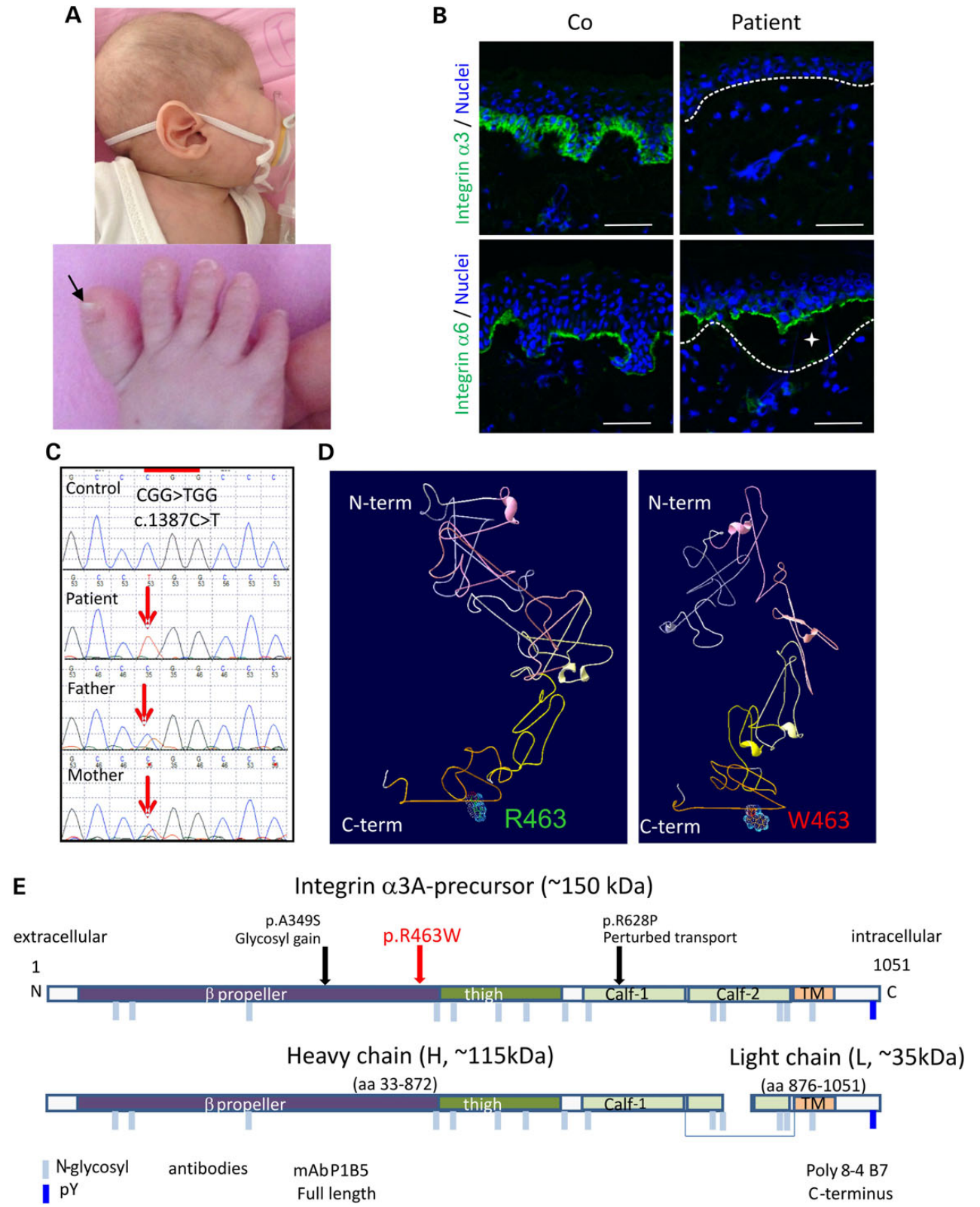

Figure 3. Clinical and molecular findings. (**A**) The patient had fine sparse scalp hair and mild toenail dystrophy. (**B**) Immunofluorescence staining of skin sections shows integrin α3 at the periphery of basal keratinocytes in the skin from a healthy control (Co) and lack of immunoreactivity in the patient's skin. Integrin α6 is distributed in a linear manner at the dermal–epidermal junction in control, and at the roof of the junctional blister (asterisk) in the patient skin. Bars = 50 μm. (**C**) Partial sequence of *ITGA3* exon 10 reveals the mutation c.1387C>T, p.R463W in a homozygous state in the patient and in a heterozygous state in each of his parents. (**D**) The tertiary structures were modeled. Note significant alteration of the conformation in the mutant (W463) compared with the wild type (R463). The seven FG-GAP repeats of the β-propeller domain are depicted in distinct colors. (**E**) Schematic representation of the integrin α3A precursor form and mature form with heavy and light chains. Domains, glycosylation and phosphorylation sites, as well as human missense mutations, are depicted. In the lower part, the epitopes of the antibodies used in this study are indicated.

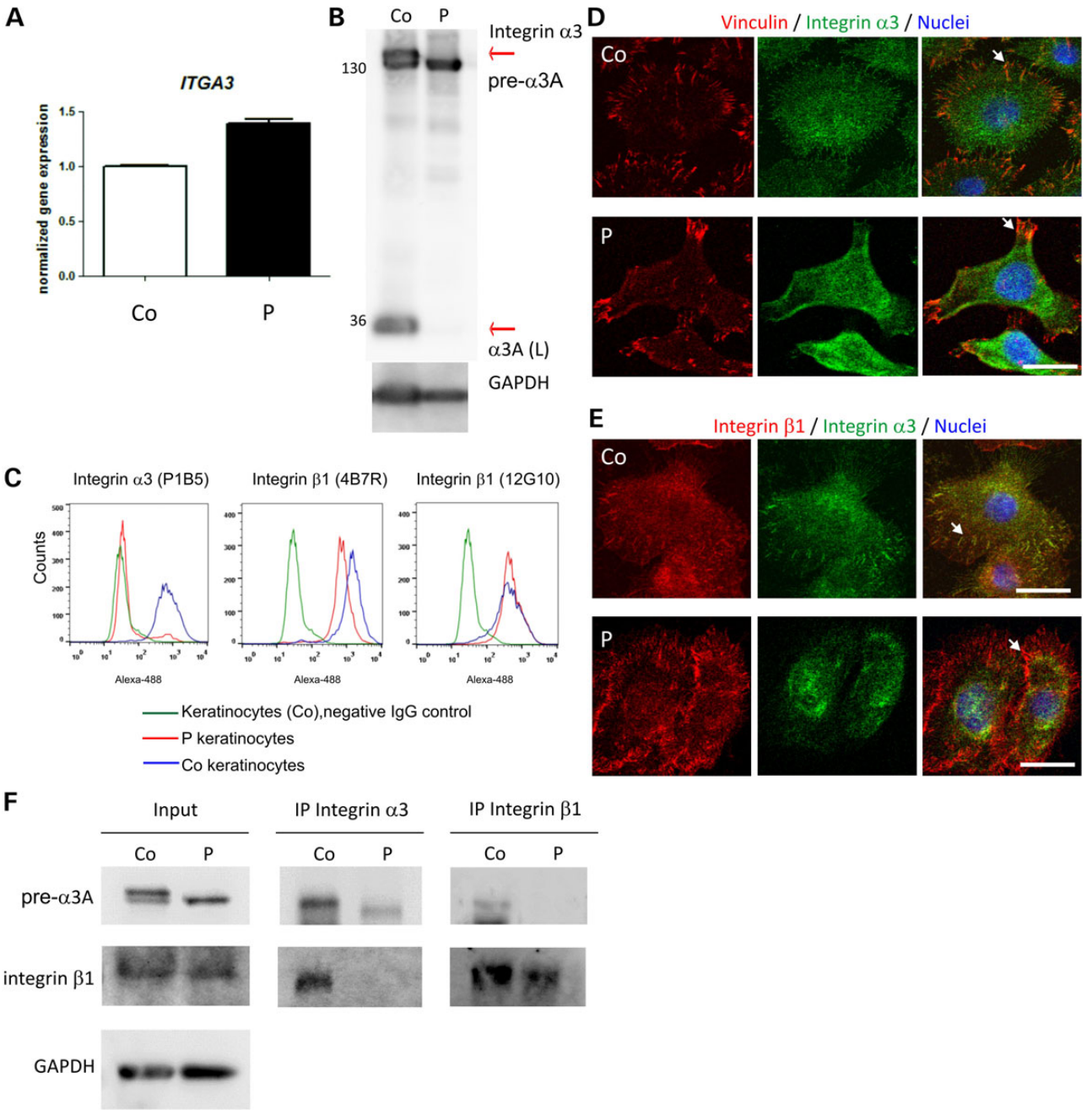

Figure 4. Consequences of the integrin α3 mutation p.R463W. **(A)** Quantitative real-time PCR demonstrates ~1.5-fold upregulation of the *ITGA3* mRNA in the patient's cells (P) compared with the control (Co). **(B)** Immunoblot analysis of cell lysates obtained from cultured keratinocytes with the antibody 8-4 B7 to integrin α3 reveals pre-α3A and the light chain in the control sample (Co); note the absence of the double band for pre-α3A and of the α3A light chain (L) in the patient's sample (P) (red arrows). Loading is shown by GAPDH staining. On the left side, the molecular weight is indicated in kilodalton. **(C)** Cell surface expression of integrin α3 (clone P1B5) and of both, total and activated integrin β1 (clones 4B7R and 12G10, respectively), was determined by flow cytometry. Green indicates the signal obtained from cells incubated only with the secondary antibody. **(D)** Immunofluorescence staining and confocal microscopy of integrin α3 with vinculin. Vinculin and integrin α3 immunostaining is visible as fine spikes in control cells. Note the altered distribution of vinculin containing focal adhesions and cytoplasmic accumulation of mutant integrin α3 in the patient's keratinocytes. **(E)** Confocal microscopy demonstrates the distribution of integrin β1 and integrin α3 at focal adhesions in control cells and cytoplasmic accumulation of mutant integrin α3 in the patient's keratinocytes. For all panels bar = 20 µm. **(F)** α3 and β1 integrins were immunoprecipitated (IP) from lysates of control and patient keratinocytes, and integrin α3 and β1 subunits were detected by immunoblotting. Loading in the input is shown by GAPDH.

keratinocytes derived from the patient, we noticed cytoplasmic accumulation and partial co-localization of mutant integrin α3 with calnexin and single co-localization signals with Golgin-97 (Fig. 5B). Hence, we cannot exclude a possible transport of the mutant integrin α3 from ER to Golgi. Moreover, both calnexin and Golgin-97 protein levels were increased in the patient compared with the control cells (Fig. 5C). Calnexin is a chaperone protein that is involved in ER retention and folding of nascent glycoproteins. Both precursors, of α and β integrin subunits, undergo complex folding and associate with calnexin to ensure

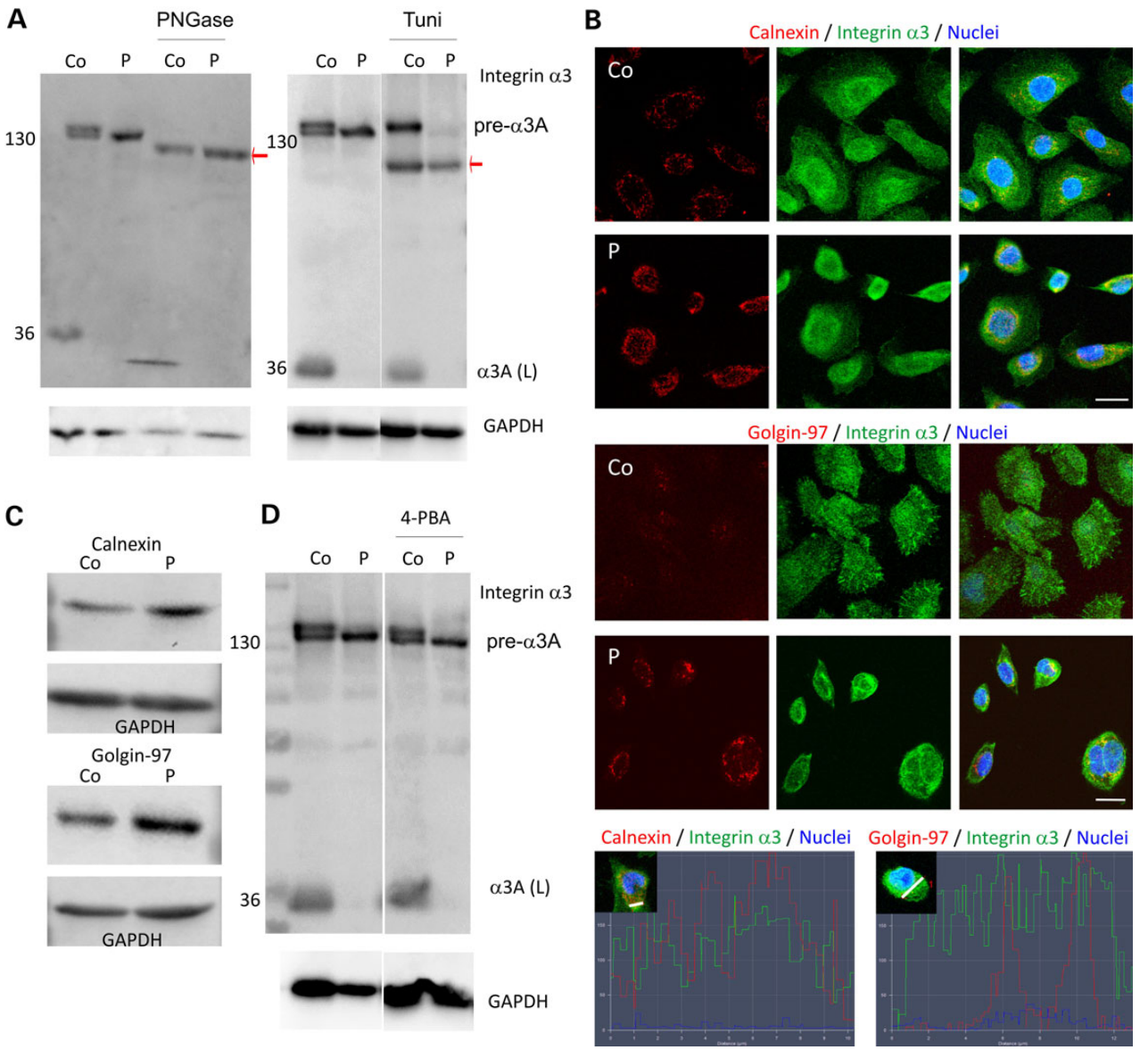

Figure 5. Disturbed processing of mutant integrin α3. **(A)** Immunoblot analysis of cell lysates obtained from cultured keratinocytes without treatment, or after treatment with PNGase, or tunicamycin (Tuni) is shown. Arrows point to the deglycosylated forms of pre-α3A. **(B)** Immunofluorescence staining and confocal microscopy of control (Co) and patient (P) keratinocytes with antibodies against to integrin α3 and calnexin or Golgin-97. The lowest panels demonstrate partial co-localization of mutant integrin α3 with calnexin and Golgin-97 in the patient's cells. The areas used in co-localization studies are labeled in white. For all panels bar = 20 μm. **(C)** Immunoblot analysis of Co and P cell lysates with antibodies to calnexin and Golgin-97. Note increased levels of these proteins in the patient's sample compared with the control. **(D)** Immunoblot analysis of cell lysates obtained from cultured keratinocytes without addition, or with 4-PBA shows no significant changes after treatment. For all immunoblots, loading is shown by GAPDH staining. On the left side, the molecular weight is indicated in kilodalton.

the proper conformation before the transport to the Golgi (20). Golgin-97 is involved in early endosome/recycling endosome-trans-Golgi network retrograde transport and has been proposed to tether early endosome/recycling endosome-derived vesicles (21). The increased levels of calnexin and Golgin-97 observed in the patients' keratinocytes may reflect cellular responses to the abnormal processing and transport of the mutant integrin. In the attempt to evade quality control mechanisms in the ER and rescue the processing of the misfolded mutant integrin α3, the patient's cells were incubated with the chemical chaperone, 4-phenylbutyrate (4-PBA). However, this treatment did not induce the cleavage and formation of the mature light chain of mutant integrin α3 (Fig. 5D).

Discussion

ILNEB is a rare autosomal recessive multiorgan disorder, first described in 2012 (1), which remains probably underrecognized. The clinical features consist of early onset interstitial lung disease, congenital nephrotic syndrome and skin fragility, but the full spectrum of clinical manifestations is still poorly characterized, and genotype–phenotype correlations are elusive. Here, we report on a case with solely interstitial lung disease and nephrotic syndrome and illuminate the underlying molecular defect. To the best of our knowledge, we disclosed a yet unreported homozygous *ITGA3* mutation leading to an amino acid substitution in the extracellular β-propeller domain of integrin α3. *In silico*

predictions indicated that the presence of tryptophan at the position 463, instead of an arginine, affects folding of this domain but not N-glycosylation or phosphorylation. Cell biological and protein chemical assays performed with authentic keratinocytes derived from the patient, bearing the naturally occurring genetic defect demonstrated that this predicted misfolding interfered with the complex processing of integrin α3 and prevented its targeting to the cell membrane.

The consequences of the integrin α3 mutation p.R463W could not be easily anticipated. Intriguingly, in the same codon, another variant, c.1388G>A, p.R463Q is referenced in dbSNP 141 (rs185439534) with a very low minor allele frequency, of 0.0006. This could also represent a rare pathogenic variant, as suggested by *in silico* predictions (PolyPhen2 Score 1, Mutation Taster score 0.573). Our experimental results demonstrate that the mutant integrin α3 is expressed in the keratinocytes of the patient at levels comparable with the control cells, but the mutation prevents correct processing of N-linked oligosaccharides and maturation by cleavage into light and heavy chains in the Golgi. Consequently, authentic mutant integrin α3 accumulates in the cells, and is not targeted to the membrane. Intriguingly, in the patient's keratinocytes the β1 subunit, the physiological heterodimerization partner of α3, was detected on the surface by flow cytometry and visualized at focal adhesions by confocal microscopy, suggesting that when α3 is not functional and does not heterodimerize with β1, other αβ1 complexes are built and utilized (own unpublished data). In this respect, Margadant *et al.* have shown that integrin α6 forms heterodimers with β1 and compensates in part for the lack of integrin α3 (13), or α2 was proposed to compensate (22), whereas in other models, neither of this was the case (23).

In our case, blocking of ubiquitination and proteosomal degradation moderately increased the α3 amount in the patient's keratinocytes, at levels comparable with the control (not shown), suggesting that protein degradation does not significantly contribute to the disease mechanisms. Since 4-PBA has been shown to reduce protein mislocalization in diseases such as cystic fibrosis (24,25), we tested its effects on mutant integrin α3, but found no evidence for rescue of the defective processing of this particular mutant.

These findings point to the severe consequences of integrin α3 single amino acid substitutions and underline the critical role of folding and processing of integrins. The effects of two other integrin α3 amino acid substitutions (Fig. 3E) have been explored in recombinant systems (2,4). The mutation p.A349S was shown to induce gain of glycosylation and to disrupt heterodimerization and cell surface expression of α3β1. In mouse podocytes, in which the human mutation p.A349S was recombinantly expressed, α3 and β1 precursors accumulated in the ER and mutant α3 were ubiquitinated and proteosomally degraded (2). The other missense mutation, p.R628P in the calf-1 domain of integrin α3 was expressed in A549 human lung adenocarcinoma cells; the experimental results raised the possibility that it induces conformational perturbations of the calf-1 domain that impairs the transport from the ER to the Golgi (4).

Regarding genotype–phenotype correlations, our patient had similar pulmonary findings with the cases that were reported before, but the severity of the renal and skin involvement was attenuated (Table 1). The pulmonary findings support the diagnosis of an alveolar growth disorder in the subgroup of interstitial lung diseases. Because integrin α3 has been identified as a critical regulator of epithelial–mesenchymal transition and tissue remodeling in response to injury (10,26), recurrent lung infections and respiratory failure developed on the basis of distorted morphogenesis (8) characterized by impaired alveolarization seem to be the most common cause of death in these patients. Renal findings were different from the other reports, because our case has never necessitated peritoneal dialysis and renal failure did not develop during his clinical observation. Furthermore, abdominal ultrasonography showed crossed fused renal ectopia, a rare congenital malformation, in which both kidneys are located on the same side and are fused, with two separate ureters arising from the respective kidneys (27). This finding strongly supports a recently published hypothesis that integrin α3 is not merely a passive anchor for renal extracellular matrix proteins, as predicted by mouse models, but is required for proper nephrogenesis (3). Finally, although there was no clinical evidence for cutaneous fragility, the analysis of a skin sample and of the keratinocytes of the patient, critically contributed to the elucidation of the molecular basis of the disease in our case.

Materials and Methods

Human tissues

After informed consent, skin and lung samples and EDTA-blood were obtained from the patient and from his parents, respectively. The study was approved by the Ethics Committee of the University of Freiburg.

Morphological analyses of the lung and the skin

For histopathological examination using light microscopy, lung and skin biopsy specimens were embedded in paraffin, and the sections were stained with hematoxylin and eosin by standard procedures. Indirect immunofluorescence staining of the patient's and control skin was performed on 5 μm cryosections, which were air dried and incubated with primary antibodies at 4°C overnight. For immunofluorescence antigen mapping, a panel of antibodies was used, as described before (1). For integrin α3, the primary antibody P1B5 (Millipore, Darmstadt, Germany) was used. The secondary antibody was Alexa-488 anti-mouse IgG. Nuclei were stained with DAPI (Millipore, Temecula, CA, USA). Stained sections were observed with a confocal laser-scanning microscope (LSM510, Carl Zeiss, Jena, Germany).

Cell culture and treatments

Normal skin specimens were obtained after informed written consent from an individual who underwent surgery, and used for isolation of cells. A part of the patient's skin obtained for diagnostic purposes was used to isolate keratinocytes, as described (28). Keratinocyte cell lines were generated by immortalization with the HPV E6E7 genes (the construct is a kind gift of Dr Fernando Larcher) (17,29) and cultured in keratinocyte growth medium (KGM) (Invitrogen, Karlsruhe, Germany).

Keratinocytes were incubated with KGM containing 1 μg/ml tunicamycin or only with KGM for 16 h (Sigma, Taufkirchen, Germany) before cell lysates were collected for the immunoblotting analysis. For the study of phosphorylation and glycosylation, cell lysates extracted from the control and patient keratinocytes were treated with 800 units lambda phosphatase (NEB, MA, USA) for 45 min at room temperature or with *N*-glycanase overnight in 37°C (PNGase, NEB); cell lysates were collected and analyzed by immunoblotting. In other sets of experiments, keratinocytes were cultured with 1–15 mM 4-PBA (Sigma, Germany) for 48 h, with 100 nM MG-132 (Calbiochem, La Jolla, CA, USA) for 6 h or with 200 μM *p*-tosyl-L-arginine methyl ester-HCl (TAME-HCL) (Sigma) for 1 h. After the indicated time points, cells were lysed as described below.

Immunofluorescence staining of cells

Cells were seeded on uncoated coverslips and allowed to grow for 2 days; thereafter, they were fixed and processed as described (17). Primary antibodies were against: integrin α3 (8-4 B7, kind gift of Dr M. DiPersio), vinculin (7F9, Chemicon), β1 integrin (4B7R, Abcam), calnexin (Abcam) and Golgin-97 (Molecular Probes, Leiden, The Netherlands). The secondary antibodies were Alexa-488 anti-mouse IgG AND Alexa-594 anti-rabbit IgG (both Invitrogen, Darmstadt, Germany). Nuclei were visualized with DAPI. Images were captured by laser-scanning confocal microscopy (ZEN 2010, Carl Zeiss) or using immunofluorescence microscopy (Zeiss Axio Imager, Zeiss, Germany). The pictures were analyzed with the software ImageJ or ZEN 2012 black (3–4D analysis, visualization and measurement) (6) (Carl Zeiss).

Mutation detection and bioinformatics

Genomic DNA was extracted from EDTA-blood using QIAmp® DNA mini kit (Qiagen, Hilden, Germany). Exon/intron boundaries of *ITGA3* were amplified by PCR as described (1). DNA sequences were compared with the reference sequence from NCBI Entrez Nucleotide database (*ITGA3* NC_000017.11) using Mutation Surveyor™ DNA variant analysis software (version 2.61 Softgenetics, State College, PA, USA).

Prediction of the consequences of the sequence variants was performed with PolyPhen-2 (http://genetics.bwh.harvard.edu/pph2/) and Mutation Taster (http://www.mutationtaster.org/).

Prediction of posttranslation modifications, glycosylation and phosphorylation were performed using http://www.cbs.dtu.dk/. Ubiquitination prediction was performed by using http://www.ubpred.org/. The tertiary structure of a sequence spanning amino acids 80–481 of wild-type and mutant integrin α3 was modeled using http://scratch.proteomics.ics.uci.edu (16).

RNA extraction and qPCR

Total RNA was isolated from the keratinocytes of the patient and of a normal control using RNAeasy® FFPE kit (Qiagen), transcribed into cDNA (Fermentas, St. Leon-Rot, Germany) and subjected to quantitative real-time PCR using iQ™ SYBR® Green Supermix and Biorad CFX96 Real-Time PCR Detection System (both Bio-Rad, Munich, Germany). Primers for *ITGA3* were: forward—CTGGTGCTGTGTACCTGTGC and reverse—GCTGGTCTT CTGACCCTGAC. Primers for *GAPDH* were: forward—CGAGATC CCTCCAAAATCAA and reverse—TTCTAGACGGCAGGTCAGGT. The data were analyzed using the Bio-Rad CFX Manager Software (version 1.5).

Protein extraction and immunoblotting

Confluent cell monolayers were lysed with a buffer containing 25 mM Tris–HCl, pH 7.5, 100 mM NaCl, 1% NP-40, 1 mM PEFA-Bloc, 10 mM EDTA and protease inhibitor cocktail (28). For immunoblotting, equal amounts of proteins were separated on 8–10% SDS–PAGE under reducing conditions and immunoblotted. The membranes were incubated with primary antibodies overnight at 4°C, followed by incubation with secondary antibodies. Primary antibodies were against integrin α3 C-terminus (8-4 B7, kind gift of Dr M. DiPersio), calnexin (Abcam), Golgin-97 (Molecular Probes, Leiden, The Netherlands) and GAPDH (clone 6C5, Millipore) to control loading. Visualization followed with the ECL Plus system (Amersham) and the Fusion system (PeQlab, Germany).

Flow cytometry

For each analysis, 2×10^5 cells were trypsinized, washed twice with PBS and then incubated with the antibody P1B5 to detect integrin α3 and with 4B7R and 12G10 to detect β1 integrin at room temperature for 15 min. 4B7R was raised against the full-length human integrin β1 and detects the total protein amount. 12G10 has been shown to recognize a small sub-region of the βl subunit, residues 207–218, and detects the active conformation of β1 (30,31). After washing with PBS containing 1% BSA and 0.05% NaN_3, the cells were incubated with FITC conjugated $F(ab')_2$ goat anti-mouse IgG(H+C) antibody (Immunotech, PN, USA) for further 15 min. In a parallel experiment, isotype controls were used. Flow cytometry acquisition was performed using the BD FACSCalibur (BD Biosciences, Oxford, UK).

Coimmunoprecipitation

Coimmunoprecipitation assays were carried out using the Pierce® Co-IP Kit (Rockford, IL, USA) with the antibodies 8-4 B7 to integrin α3 and clone JB1A to integrin β1 (Millipore), or the corresponding preimmune sera. The cell monolayers were lysed with the lysis buffer (0.025 M Tris, 0.15 M NaCl, 0.001 M EDTA, 1% NP-40, 5% glycerol, pH 7.4). After centrifugation at 13 000*g* for 10 min, the supernatant was transferred to the resin and incubated at 4°C for 2 h. The samples were washed and eluted. The elution samples were resolved in SDS–PAGE and immunoblotted with 8-4 B7 to integrin α3 and JB1A to integrin β1. GAPDH was used as a loading control in the input.

Acknowledgements

In particular, we thank the family of the patient. The authors thank Juna Leppert for excellent technical assistance. We thank Prof. Megan Dishop for reviewing the slides of the lung biopsy. We thank Dr Michael DiPersio (Albany Medical College, USA) for providing reagents, Dr Fernando Larcher (CIEMAT-CIBER, Madrid, Spain) for the E6E7 construct and Dr Claus-Werner Franzke (University Freiburg) for helpful discussions. The contribution of the 'Center for Human Genetics Freiburg' led by Dr Jürgen Kohlhase as a sequencing facility is acknowledged.

Conflict of Interest statement. None declared.

Funding

Y.H. was supported by the Else-Kröner Fresenius foundation and C.H. by the Deutsche Forschungsgemeinschaft (DFG) CRC/SFB 1140. C.P. is a fellow of the Spemann graduate school.

References

1. Has, C., Sparta, G., Kiritsi, D., Weibel, L., Moeller, A., Vega-Warner, V., Waters, A., He, Y., Anikster, Y., Esser, P. *et al.* (2012) Integrin alpha3 mutations with kidney, lung, and skin disease. *N. Engl. J. Med.*, **366**, 1508–1514.
2. Nicolaou, N., Margadant, C., Kevelam, S.H., Lilien, M.R., Oosterveld, M.J., Kreft, M., van Eerde, A.M., Pfundt, R., Terhal, P.A., van der Zwaag, B. *et al.* (2012) Gain of glycosylation in integrin alpha3 causes lung disease and nephrotic syndrome. *J. Clin. Invest.*, **122**, 4375–4387.
3. Shukrun, R., Vivante, A., Pleniceanu, O., Vax, E., Anikster, Y., Dekel, B. and Lotan, D. (2014) A human integrin-alpha3 mutation confers major renal developmental defects. *PLoS ONE*, **9**, e90879.

4. Yamada, M. and Sekiguchi, K. (2013) Disease-associated single amino acid mutation in the calf-1 domain of integrin alpha3 leads to defects in its processing and cell surface expression. *Biochem. Biophys. Res. Commun.*, **441**, 988–993.
5. Winograd-Katz, S.E., Fassler, R., Geiger, B. and Legate, K.R. (2014) The integrin adhesome: from genes and proteins to human disease. *Nat. Rev. Mol. Cell. Biol.*, **15**, 273–288.
6. Margadant, C., Charafeddine, R.A. and Sonnenberg, A. (2010) Unique and redundant functions of integrins in the epidermis. *FASEB J.*, **24**, 4133–4152.
7. Sachs, N. and Sonnenberg, A. (2013) Cell-matrix adhesion of podocytes in physiology and disease. *Nat. Rev. Nephrol.*, **9**, 200–210.
8. Kreidberg, J.A., Donovan, M.J., Goldstein, S.L., Rennke, H., Shepherd, K., Jones, R.C. and Jaenisch, R. (1996) Alpha 3 beta 1 integrin has a crucial role in kidney and lung organogenesis. *Development*, **122**, 3537–3547.
9. Sachs, N., Kreft, M., van den Bergh Weerman, M.A., Beynon, A. J., Peters, T.A., Weening, J.J. and Sonnenberg, A. (2006) Kidney failure in mice lacking the tetraspanin CD151. *J. Cell. Biol.*, **175**, 33–39.
10. Kim, K.K., Wei, Y., Szekeres, C., Kugler, M.C., Wolters, P.J., Hill, M.L., Frank, J.A., Brumwell, A.N., Wheeler, S.E., Kreidberg, J.A. *et al.* (2009) Epithelial cell alpha3beta1 integrin links beta-catenin and Smad signaling to promote myofibroblast formation and pulmonary fibrosis. *J. Clin. Invest.*, **119**, 213–224.
11. DiPersio, C.M., Hodivala-Dilke, K.M., Jaenisch, R., Kreidberg, J.A. and Hynes, R.O. (1997) Alpha3beta1 integrin is required for normal development of the epidermal basement membrane. *J. Cell Biol.*, **137**, 729–742.
12. Longmate, W.M., Monichan, R., Chu, M.L., Tsuda, T., Mahoney, M.G. and DiPersio, C.M. (2014) Reduced fibulin-2 contributes to loss of basement membrane integrity and skin blistering in mice lacking integrin alpha3beta1 in the epidermis. *J. Invest. Dermatol.*, **134**, 1609–1617.
13. Margadant, C., Raymond, K., Kreft, M., Sachs, N., Janssen, H. and Sonnenberg, A. (2009) Integrin alpha3beta1 inhibits directional migration and wound re-epithelialization in the skin. *J. Cell. Sci.*, **122**, 278–288.
14. DiPersio, C.M., van der Neut, R., Georges-Labouesse, E., Kreidberg, J.A., Sonnenberg, A. and Hynes, R.O. (2000) Alpha3beta1 and alpha6beta4 integrin receptors for laminin-5 are not essential for epidermal morphogenesis and homeostasis during skin development. *J. Cell. Sci.*, **113**, 3051–3062.
15. Conti, F.J., Rudling, R.J., Robson, A. and Hodivala-Dilke, K.M. (2003) Alpha3beta1-integrin regulates hair follicle but not interfollicular morphogenesis in adult epidermis. *J. Cell. Sci.*, **116**, 2737–2747.
16. Cheng, J., Randall, A.Z., Sweredoski, M.J. and Baldi, P. (2005) SCRATCH: a protein structure and structural feature prediction server. *Nucleic Acids Res.*, **33**, W72–W76.
17. Has, C., Herz, C., Zimina, E., Qu, H.Y., He, Y., Zhang, Z.G., Wen, T.T., Gache, Y., Aumailley, M. and Bruckner-Tuderman, L. (2009) Kindlin-1 is required for RhoGTPase-mediated lamellipodia formation in keratinocytes. *Am. J. Pathol.*, **175**, 1442–1452.
18. DiPersio, C.M., Shah, S. and Hynes, R.O. (1995) Alpha 3A beta 1 integrin localizes to focal contacts in response to diverse extracellular matrix proteins. *J. Cell. Sci.*, **108**, 2321–2336.
19. Lissitzky, J.C., Luis, J., Munzer, J.S., Benjannet, S., Parat, F., Chretien, M., Marvaldi, J. and Seidah, N.G. (2000) Endoproteolytic processing of integrin pro-alpha subunits involves the redundant function of furin and proprotein convertase (PC) 5A, but not paired basic amino acid converting enzyme (PACE) 4, PC5B or PC7. *Biochem. J.*, **346**, 133–138.
20. Lenter, M. and Vestweber, D. (1994) The integrin chains beta 1 and alpha 6 associate with the chaperone calnexin prior to integrin assembly. *J. Biol. Chem.*, **269**, 12263–12268.
21. Lu, L., Tai, G. and Hong, W. (2004) Autoantigen Golgin-97, an effector of Arl1 GTPase, participates in traffic from the endosome to the trans-Golgi network. *Mol. Biol. Cell*, **15**, 4426–4443.
22. Wen, T., Zhang, Z., Yu, Y., Qu, H., Koch, M. and Aumailley, M. (2010) Integrin alpha3 subunit regulates events linked to epithelial repair, including keratinocyte migration and protein expression. *Wound Repair Regen.*, **18**, 325–334.
23. Hodivala-Dilke, K.M., DiPersio, C.M., Kreidberg, J.A. and Hynes, R.O. (1998) Novel roles for alpha3beta1 integrin as a regulator of cytoskeletal assembly and as a trans-dominant inhibitor of integrin receptor function in mouse keratinocytes. *J. Cell. Biol.*, **142**, 1357–1369.
24. Rubenstein, R.C. and Zeitlin, P.L. (1998) A pilot clinical trial of oral sodium 4-phenylbutyrate (Buphenyl) in deltaF508-homozygous cystic fibrosis patients: partial restoration of nasal epithelial CFTR function. *Am. J. Respir. Crit. Care Med.*, **157**, 484–490.
25. Rubenstein, R.C., Egan, M.E. and Zeitlin, P.L. (1997) In vitro pharmacologic restoration of CFTR-mediated chloride transport with sodium 4-phenylbutyrate in cystic fibrosis epithelial cells containing delta F508-CFTR. *J. Clin. Invest.*, **100**, 2457–2465.
26. Kim, Y., Kugler, M.C., Wei, Y., Kim, K.K., Li, X., Brumwell, A.N. and Chapman, H.A. (2009) Integrin alpha3beta1-dependent beta-catenin phosphorylation links epithelial Smad signaling to cell contacts. *J. Cell. Biol.*, **184**, 309–322.
27. Patel, T.V. and Singh, A.K. (2008) Crossed fused ectopia of the kidneys. *Kidney Int.*, **73**, 662.
28. Herz, C., Aumailley, M., Schulte, C., Schlotzer-Schrehardt, U., Bruckner-Tuderman, L. and Has, C. (2006) Kindlin-1 is a phosphoprotein involved in regulation of polarity, proliferation, and motility of epidermal keratinocytes. *J. Biol. Chem.*, **281**, 36082–36090.
29. Sprenger, A., Kuttner, V., Biniossek, M.L., Gretzmeier, C., Boerries, M., Mack, C., Has, C., Bruckner-Tuderman, L. and Dengjel, J. (2010) Comparative quantitation of proteome alterations induced by aging or immortalization in primary human fibroblasts and keratinocytes for clinical applications. *Mol. Biosyst.*, **6**, 1579–1582.
30. Takada, Y. and Puzon, W. (1993) Identification of a regulatory region of integrin beta 1 subunit using activating and inhibiting antibodies. *J. Biol. Chem.*, **268**, 17597–17601.
31. Mould, A.P., Garratt, A.N., Askari, J.A., Akiyama, S.K. and Humphries, M.J. (1995) Identification of a novel anti-integrin monoclonal antibody that recognises a ligand-induced binding site epitope on the beta 1 subunit. *FEBS Lett.*, **363**, 118–122.